We are IntechOpen, the world's leading publisher of Open Access books Built by scientists, for scientists

4,800
Open access books available

122,000
International authors and editors

135M
Downloads

Our authors are among the

154
Countries delivered to

TOP 1%
most cited scientists

12.2%
Contributors from top 500 universities

CLARIVATE ANALYTICS BOOK CITATION INDEX INDEXED

WEB OF SCIENCE™

Selection of our books indexed in the Book Citation Index in Web of Science™ Core Collection (BKCI)

Interested in publishing with us?
Contact book.department@intechopen.com

Numbers displayed above are based on latest data collected.
For more information visit www.intechopen.com

21

Photonic Millimeter-wave Generation and Distribution Techniques for Millimeter/sub-millimeter Wave Radio Interferometer Telescope

Hitoshi Kiuchi[1] and Tetsuya Kawanishi[2]
[1]*National Astronomical Observatory of Japan*
[2]*National Institute of Information and Communications Technology*
Japan

1. Introduction

In the field of high-frequency radio interferometer, Atacama Large Millimeter/sub-millimeter Array (ALMA), its highest receiving frequency reaches 950 GHz. To receive such high frequencies, a higher reference frequency for frequency conversion is required (as much as over 100 GHz). To maintain signal coherency, this reference signal has to be highly stable. To address these issues, we have developed a new method to generate and transmit a reference signal in the form of frequency difference between two coherent light waves. One method to generate two optical signals is producing them from a pair of laser sources using optical phase lock loop for feed back control (Cliche & Shillue (2006)), however, optical phase lock loop also requires a stable laser source. A good alternative method to the optical phase lock scheme is the lithium niobate ($LiNbO_3$) Mach-Zehnder optical modulator which is capable of generating two highly stable optical signals (upper sideband and lower sideband components) by applying a sinusoidal microwave signal to an input laser signal. Compared to the current optical phase lock scheme, the Mach-Zehnder modulator has significant advantages in terms of stability (free from the influence of the input laser stability), robustness to mechanical vibration and acoustic noise, and capability of maintaining polarization state of the input laser. During the signal transmission through the fiber cable, the cable length delay fluctuation is caused together with polarization mode dispersion, which will impact the performance of coherent signal distribution. We have developed the phase stabilizer using the dual difference round-trip phase measurement method with Michelson's interferometer. The roundtrip phase measurement is performed on each lightwave signal separately. The Round-trip phase measurement method is helpful for successful delay compensation of the microwave signal which is converted from the two coherent optical signals by a photo mixer. The two transmitted optical signals require phase stability better than 10^{-13} (1sec) in white phase noise in the Allan standard deviation for ALMA project.

2. Astronomical requirements

The modulation signal is transmitted via one optical fiber in the form of frequency difference between two coherent optical signals. These two optical signals are subsequently

Source: Advances in Lasers and Electro Optics, Book edited by: Nelson Costa and Adolfo Cartaxo,
ISBN 978-953-307-088-9, pp. 838, April 2010, INTECH, Croatia, downloaded from SCIYO.COM

converted into millimeter-wave signal by the photo mixer at the remote antenna. The region from 27 GHz to 122 GHz (Table 1) is used for operational frequency for ALMA 10-band receivers. The two-tone generator requires polarization maintaining capability as well as mechanical vibration and acoustic noise robustness to avert the impact of the polarization effect on the photo-mixer and that of the polarization mode dispersion on the transmission fiber.

	Reference freq. range (GHz)	Local freq. range (GHz)
Band 1	27.3-33.0	27.3-33.0
Band 2	79.0-94.0	79.0-94.0
Band 3	92.0-108.0	92.0-108.0
Band 4	68.5-75.5	137.0-151.0
Band 5	87.5-99.5	175.0-199.0
Band 6	74.3-87.7	223.0-263.0
Band 7	94.3-121.7	283.0-365.0
Band 8	79.4-97.6	397.0-488.0
Band 9	102.3-118.0	614.0-708.0
Band 10	88.8-104.2	799.0-938.0

Table 1. Required frequency range.

2.1 Phase noise

The behavior of phase noise can be analyzed by the Allan standard deviation (Allan (1966; 1976)). The frequency instability is the frequency change induced by internal or external factors within a given time interval. In other words, the frequency instability is defined as the degree to which the output frequency remains constant over a specified period of time. Characteristics of phase noises (Healey (1972)) are shown in Fig. 1.

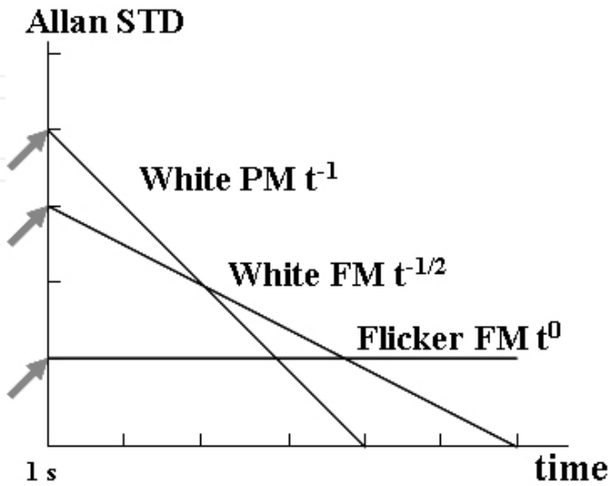

Fig. 1. Phase noises of a highly stable signal.

Noises are classified into the following five types according to the noise generation mechanism: white phase modulation noise (τ^{-1}), flicker phase modulation noise (τ^{-1}), white frequency modulation noise ($\tau^{-1/2}$), flicker frequency modulation noise (τ^{0}) and Random Walk frequency modulation noise ($\tau^{1/2}$) (Healey (1972)). Some of these noises are generated by electronic equipment or by changes in the environment (such as temperature change).

2.2 Estimation of coherence loss and time error by the Allan standard deviation

The coherence loss due to the instability in the frequency standard for *T-sec* integration times is estimated Eq. (1) (Rogers & Moran (1981); Rogers et al. (1984); Kawaguchi (1983)).

$$L_c = \omega_o^2[\frac{\alpha_p}{6} + \frac{\alpha_f}{12}T + \frac{\sigma_y^2}{57}T^2] \tag{1}$$

where
L_c the loss of coherence,
ω_0 the angular frequency of local oscillator,
α_p the Allan variance [(*standard deviation*)^2] of white phase noise at l sec,
α_f the Allan variance [(*standard deviation*)^2] of white frequency noise at l sec,
σ_y^2 the constant Allan variance [(*standard deviation*)^2] of flicker frequency noise,
T the integration time [sec].

Coherence loss and time error are calculated by the Allan standard deviation. One of the stability measurement methods in time domain is the Dual-Mixer Time Difference (DMTD) method (Allan (1976)) which is adopted by NIST (National Institute of Standards and Technology, USA), NICT (National Institute of Communications and Technology, Japan) and other time/frequency standard institutes. Using this method, the phase stability of a device-undertest can be obtained without influence of unstable local frequencies of the measurement system. The Dual-Mixer Time Difference method allows time measurements and frequency and frequency stability measurements for sample times as short as a few milliseconds or longer without dead time. Moreover, the phase noise in the measurement system can be canceled out with this method.

The total system instability is calculated by RSS (root sum square) of the Allan standard deviation of each component. Time error of phase noise is calculated as follows:

$$Time\ error = \frac{T \times \sigma_y(T\ sec)}{\sqrt{3}}$$

$$= \frac{\sigma_y(1\ sec)}{\sqrt{3}} \tag{2}$$

in white Phase Modulation noise

$$= \frac{\sigma_y(1\ sec)}{\sqrt{T}} \tag{3}$$

in white Frequency Modulation noise

$$= \frac{T \times \sigma_y(1\,sec)}{\sqrt{\ln 2}} \tag{4}$$

in flicker Frequency Modulation noise

According to the system-level technical requirements of ALMA, the instrumental delay/phase error of the 1st Local system should be 53 fs in the short time period, and the difference between 10 sec averages at intervals of 300 sec should be 17.7 fs in RMS. When these values are converted to the Allan standard deviation using Equations (2), (3), and (4), it turns out that the noises are white phase modulation noise and flicker frequency modulation noise. The short time stability of white phase modulation noise is obtained Eq. (2): $\sigma_y(\tau = 1) = 9.2 \times 10^{-14}$. Calculating from Eq. (4) and 10 seconds averaging, the required stability is $\sigma_y(\tau = 1) = 1.56 \times 10^{-16}$ (flicker phase modulation noise) in the long-time period.

3. Photonic millimeter-wave generator

In the high-extinction ratio lithium niobate ($LiNbO_3$) Mach-Zehnder intensity modulator (Izutsu et al. (1977), Izutsu et al. (1981), Kawanishi et al. (2006), Kawanishi et al. (2004a), Kawanishi et al. (2004b), Kawanishi et al. (2007), Onillon et al. (2005), Vegas et al. (2003)), the optical frequency difference between two optical signals is exactly twice (or four times) the modulation frequency, and the output signal is equivalent to FSK (frequency shift keying) spectrum. Compared to the optical phase lock scheme, the Mach-Zehnder modulator (shown in Fig. 2) has significant advantages in terms of robustness to mechanical vibration

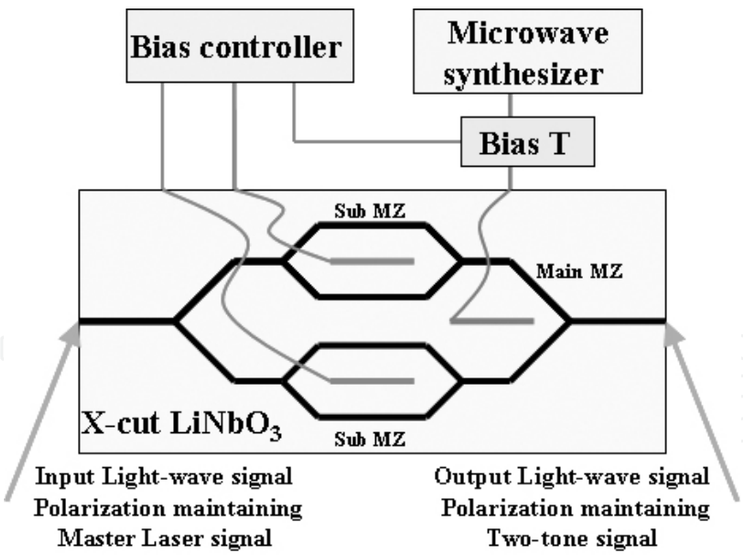

Fig. 2. Simplified structure of an optical modulator with two arms and electrodes. Optical phase of each arm is controlled by applying DC bias to the electrodes. Amplitude imbalance due to fabrication error is compensated with sub-Mach-Zehnder trimmers. When two lightwaves are in phase, the output optical signals are strengthened each other. On the other hand, when the phases of the input lightwaves are shifted, the phase-shifted lightwaves are radiated away as higher-order waves, and do not reach the optical waveguide. This is the main feature of the Mach-Zehnder modulator.

and acoustic noise, stability (free from the influence of the input laser stability), and capability of maintaining polarization state of the input laser. The Mach-Zehnder modulator is so reliable that it has been used for optical submarine cables. The estimated lifetime of the Mach-Zehnder modulator extends to several decades.
The output spectrum depends on the DC bias voltage applied to the electrodes in the Mach-Zehnder structure. The Mach-Zehnder modulator has the following two operation modes (Kawanishi et al. (2005), Kiuchi et al. (2007), Sakamoto et al. (2005)).

3.1 Operation mode

3.1.1 Null-bias point operation mode

When the bias of the Mach-Zehnder modulator is set to a minimum transmission point (nullbias point), the first-order upper side band (USB) and lower side band (LSB) components are strengthened, and the carrier is suppressed (Fig. 3). The frequency difference between the two spectral components is twice the modulation sinusoidal signal frequency. As the spectral components generated by the optical modulation are phase-locked, it is possible to construct a robust system without using any complicated feedback control technique. However, as the modulation frequency is limited by the frequency response of the modulator, the frequency upper limit of the two optical signals can not be higher than 100 GHz in the null-bias point operation mode. For this reason, the null-bias point operation mode is suitable for the low-frequency application.

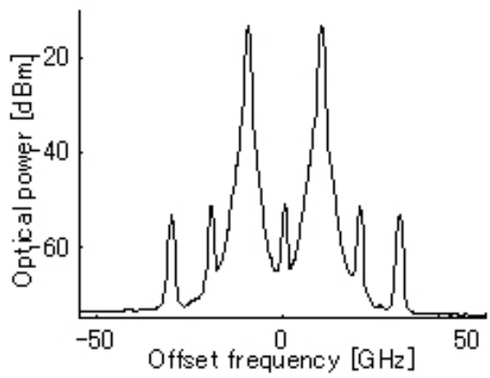

Fig. 3. When the bias of the Mach-Zehnder modulator is set to a minimum transmission point (null-bias point), the first-order USB and LSB components are strengthened, and the carrier is suppressed. The frequency difference between the two spectral components is exactly twice the modulation signal frequency. Each sideband signal spectrum shows a copy of the input laser spectrum. High carrier suppression ratio of 50 dB was demonstrated by the nullbias point operation mode using the integrated Mach-Zehnder modulator with an intensity trimmer in each arm (sub-Mach-Zehnder interferometer).

3.1.2 Full-bias point operation mode

When the bias is set to a maximum transmission point (full-bias point), the second-order USB and LSB are strengthened, and the carrier is not suppressed. If the extinction ratio of the Mach-Zehnder modulator is high, undesired odd-order USB and LSB components can be successfully suppressed with this technique. When the odd-order sideband components are suppressed in this mode, the optical frequency of even-order (zero- and second-order)

components is remained (Fig. 4 left side). Eliminating the zero-order component (carrier), the remaining is a two-tone optical spectrum whose frequency is four times the modulation frequency or 4 *fm* (*fm* is the modulation frequency of the RF signal applied to the modulator). The frequency difference between the zero-order and second-order components is 2 *fm*. When 4 *fm* > 50 GHz, the frequency difference is large enough that the zero-order component can be eliminated with a conventional optical filter (Fig. 4 right side). The optical signal filtered by the optical filter is amplified by an optical amplifier. At this point, the first-order components are suppressed by the Mach-Zehnder modulator with high extinction ratio to prevent undesired spurious signals.

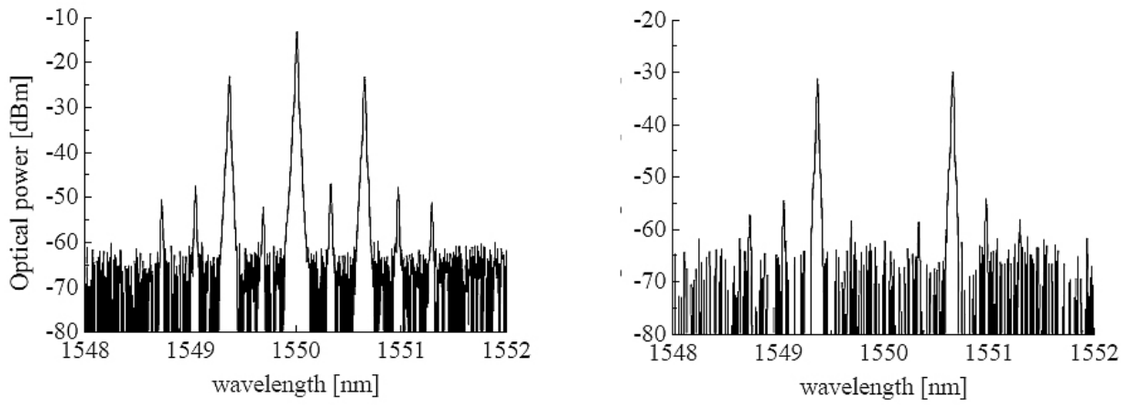

Fig. 4. When the bias of the Mach-Zehnder modulator is at full-bias point, the odd-order sideband components are suppressed. In this case, the optical frequency of even-order (zero-order and second-order) components is remained (left chart). Eliminating the zero-order component (carrier: input lightwave), the remaining is a two-tone optical spectrum whose frequency is four times the modulation frequency (right chart).

3.2 Harmonic generation process

The input light-wave is assumed to be monochromatic, and can be described by $A_{LW}e^{2\pi i f_0 t}$, where A_{LW} is the optical transmittance in the waveguide. Light-waves with RF signal can be obtained by modulation of sinusoidal RF signals into USB and LSB components using an optical intensity modulator. Assuming the RF signal is a sinusoidal signal, it is expressed as $2A_{RF}\sin(2\pi f_m t + \phi_B)$, and the optical output is expressed as shown in Eq. 7(Kawanishi et al. (2007)).

$$R = \frac{1}{2}A_{LW}e^{2\pi i f_0 t}[e^{i(A_{RF}\sin(2\pi f_m t+\phi_B/2))} + e^{-i(A_{RF}\sin(2\pi f_m t+\phi_B/2))}] \quad (5)$$

$$= \frac{1}{2}A_{LW}e^{2\pi i f_0 t}\sum_{n=-\infty}^{\infty}J_n(A_{RF})e^{2\pi i[f_0 t+nf_m t]} \times[e^{i\phi_B/2}+(-1)^n e^{-i\phi_n/2}] \quad (6)$$

$$= A_{LW} e^{2\pi i f_0 t} [\cos\frac{\phi_B}{2} \sum_{n=-\infty}^{\infty} J_{2n}(A_{RF}) e^{2\pi i [f_0 t + 2n f_m t]}$$

$$+ i \sin\frac{\phi_B}{2} \sum_{n=-\infty}^{\infty} J_{2n+1}(A_{RF}) e^{2\pi i [f_0 t + (2n+1) f_m t]}] \quad (7)$$

The output optical intensity $|R|^2$, which is detected by a high-speed photo-mixer, is expressed by Eq. 8.

$$|R|^2 \simeq |A_{LW}|^2 [J_0^2(A_{RF})\cos^2\frac{\phi_B}{2} + 2J_1^2(A_{RF})\sin^2\frac{\phi_B}{2}$$

$$-4J_0(A_{RF})J_1(A_{RF})\sin\frac{\phi_B}{2}\cos\frac{\phi_B}{2}\sin 2\pi f_m t$$

$$+2(2J_0(A_{RF})J_2(A_{RF})\cos^2\frac{\phi_B}{2}$$

$$-J_1^2(A_{RF})\sin^2\frac{\phi_B}{2})\cos(2\times 2\pi f_m t)] \quad (8)$$

where the high-order components are neglected assuming $A_{RF} \ll 1$, and the high-order components are neglected. By using Taylor's expansion of Bessel function, Eq. 9 is obtained.

$$\frac{|R|^2}{|A_{LW}|^2} = \frac{1}{2} + \frac{1-|A_{RF}|^2}{2}\cos\phi_B$$

$$-A_{RF}\sin\phi_B \sin 2\pi f_m t$$

$$+\frac{1}{2}|A_{RF}|^2 \cos\phi_B \cos(2\times 2\pi f_m t) \quad (9)$$

The intensities of the fundamental component $\sin(2\pi f_m t)$ and the second-order harmonic $\cos(2 \times 2\pi f_m t)$ can be controlled by the DC-bias ϕ_B. The fundamental and second-order components are proportional to $\sin(\phi_B)$ and $\cos(\phi_B)$, respectively. The ratio between the average power and RF signal component depends largely on the conversion efficiency from light-waves to RF signals at the photo-mixer. The ratios for the fundamental and second-order components are expressed in Eqs. 10, 11.

$$D_1 = |\frac{2A_{RF}\sin\phi_B}{1+(1-|A_{RF}|^2)\cos\phi_B}| \quad (10)$$

$$D_2 = |\frac{|A_{RF}|^2 \cos\phi_B}{1+(1-|A_{RF}|^2)\cos\phi_B}| \quad (11)$$

In the case of $\phi_B = \pi$, the even-order components in the output signal R, including the carrier components $e^{2\pi i f_0 t}$ are suppressed and the average power $|R|^2$ is reduced to minimum of

$|A_{RF}|^2/2$, where the dominant components are first-order USBs and LSBs. In the case of ϕ_B = 0, the odd-order components are suppressed, and the dominant components are zero-order and second-order USBs and LSBs.

3.3 Need for the high-extinction ratio modulator

Three Mach-Zehnder structure LN-modulator can provide high-extinction ratio (more than 55 dB) modulation signals. Simulated signals are shown in Figs. 5 and 6. High-extinction

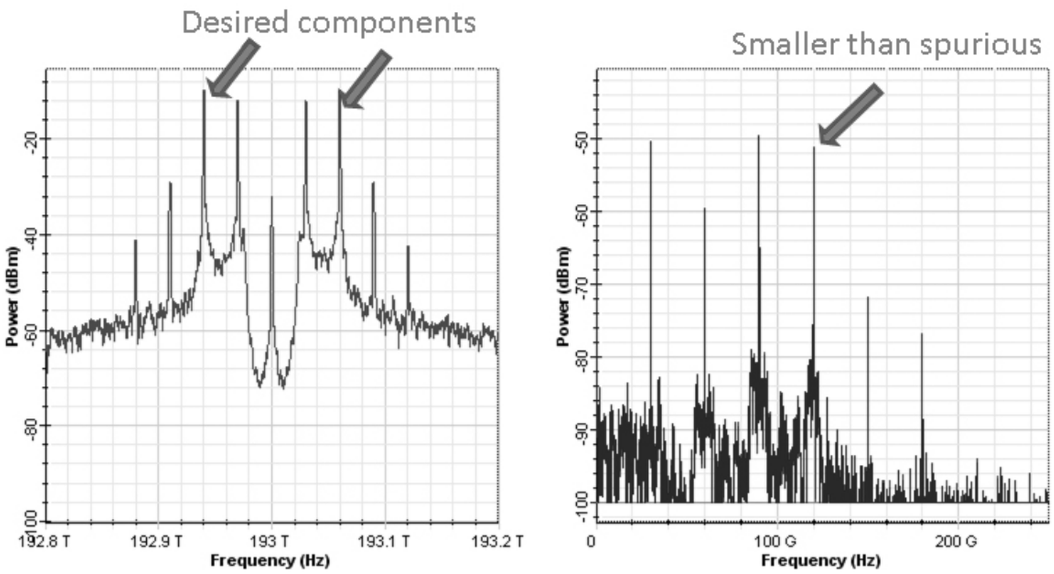

Fig. 5. Simulated low extinction ratio (20 dB) modulation signal. Optical spectrum (left) and micro wave spectrum (right).

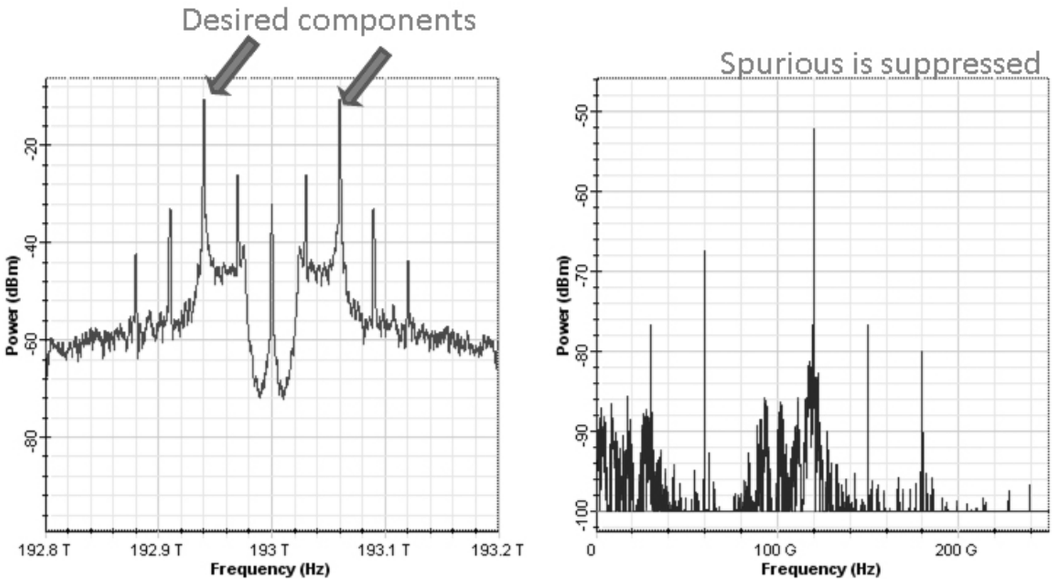

Fig. 6. Simulated high extinction ratio (50 dB) modulation signal. Optical spectrum (left) and micro wave spectrum (right).

ratio performance is effective in suppressing of excessive signals. Suppression of spurious is very important to ensure effective photonic LO signal distribution.

3.4 Stability measurement

In the case of the interferometer, we use the hydrogen maser which has the best short-term stability among existing atomic clocks as the reference signal source if necessary. There is also a method to measure the phase noise of components without using the hydrogen maser. We can estimate the total phase noise of the interferometer system, using the covariance that is obtained by; 1) measuring the phase noise of a single unit independent from the reference signal and the reference signal phase noise that is separately measured and 2) taking the root sum square of these phase noises. We should use time domain Allan standard deviation measurement with DMTD method instead of the frequency domain SSB phase noise measurement method which measures the phase noises of all signals as a whole. The Allan standard deviation in time domain is used to calculate the coherence loss and time error.

3.4.1 Time domain phase measurement method for the null-bias point operation mode

Figure 7 shows a time-domain stability measurement system to measure the differential phase between the second harmonic of the reference synthesizer and the first-order modulated signal (null-bias point operation mode). The figure shows the experimental setup of the Dual-Mixer Time Difference system (mixers, filters, and a Time Interval Analyzer: TSC-5110A) for phase noise measurement using a 22 GHz signal. The origin of the source signal is a 11 GHz synthesizer. The 11 GHz signal is used as a modulation signal, and the 22 GHz signal (spurious signal of 11 GHz, Fig. 7) is used as a reference signal (on the lower arm). These signals are coherent since the 22 GHz signal is a harmonic of the 11 GHz signal. Two coherent optical signals with 22 GHz difference are generated by optical modulation of the optical source signal using the Mach-Zehnder modulator. These two signals are subsequently converted to a 22 GHz microwave signal (on the upper arm) by the photo-

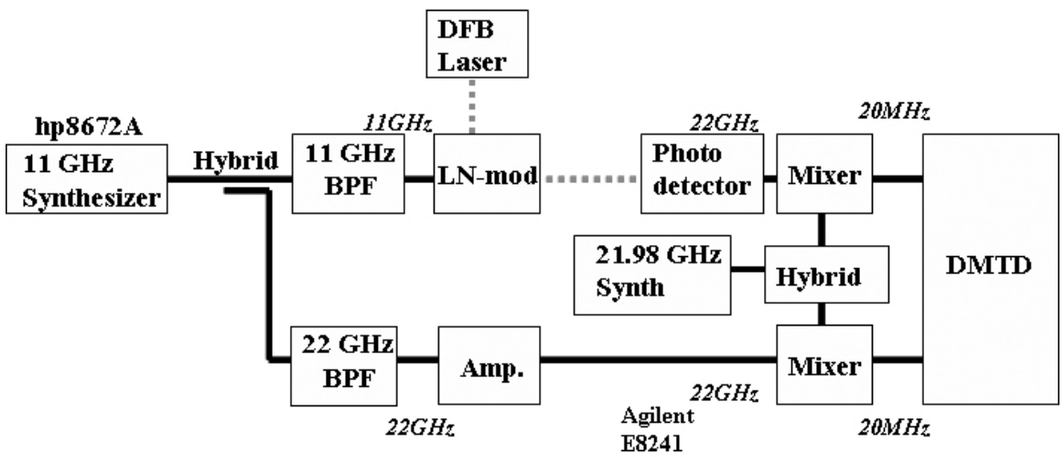

Fig. 7. Block diagram of a time-domain stability measurement system for the null-bias point operation mode (the first-order optical signal). This phase noise measurement system is free from the influence of reference signal phase noise and frequency conversion signal phase noise.

mixer. The frequencies of the two 22 GHz signals (on both arms) are converted to 20 MHz with a common 21.98 GHz signal. After these processes, the phase difference between the two 20 MHz signals is measured by the Dual-Mixer Time Difference system. In this experimental setup, the 21.98 GHz synthesizer, the hybrid, and mixers compose a kind of a Dual-Mixer Time Difference system. During these operations, the 20 MHz signals are free from the instability of the 11 GHz and 21.98 GHz synthesizers.

3.4.2 Time domain phase measurement method for the full-bias point operation mode

Figure 8 shows a time-domain stability measurement system to measure the differential phase between the multiplied (×4) reference signals and the second-order modulated signal (Full-bias point operation mode). In the case of 100 GHz measurement, the source signal is generated from the 25 GHz sinusoidal synthesizer, and the generated 25 GHz signal is used as a modulation signal and a multiplied reference signal. The microwave multiplier generates 100 GHz. Two coherent optical signals with 100 GHz difference are generated by optical modulation of the optical source signal using the Mach-Zehnder modulator. These two signals are subsequently converted to a 100 GHz microwave signal by the photo-mixer. The frequencies of the two 100 GHz signals are converted to 10 MHz by harmonic-mixers (multiplied number is 10) with a common 9.999 GHz synthesizer signal. After these processes, the differential phase between the two 10 MHz signals is measured by the Dual-Mixer Time Difference system. In this experimental setup, the 9.999 GHz synthesizer, the hybrid, and harmonic-mixers in the figure compose a kind of a common noise system. During these operations, the 10 MHz signals are free from the instability of the 25 GHz and 9.999 GHz synthesizers. The measured phase noise is the covariance of the two systems (Mach-Zehnder modulator and multiplier).
We used an NTT photo-mixer, an Uni-traveling-carrier photodiode (UTC-PD)(Hirota et al. (2001), Ito et al. (2000)). Responsibility of the photodiode is approximately 0.4 A/W. The typical output power (100 GHz) is approximately 0.5 mW.

3.5 Measured stability

To make the Dual-Mixer Time Difference method available, it is required that the phase stability of the multiplier be better than that of the Mach-Zehnder modulator, or the stability of the two systems be almost equivalent.
The results of the SSB phase noise measurement method include not only the phase noises of the LN-modulator (or multiplier) but also those of the reference signal generator (Synthesizer). Therefore the measured SSB phase noise heavily depends on the reference signal phase noise. On the other hand, the DMTD method measures differential phase noise between the measurement signal and the reference signal. In our system, the measurement signal and the reference signal are generated from the same source, which means we can offset the phase noise of the signal source, or the common noise, when obtaining the covariance between the modulator and multiplier. If the phase noises of the modulator and multiplier are almost equivalent or that of the modulator is better, we can use the obtained Allan standard deviation as the phase noise after dividing it with the square root of two. If the multiplier has much better phase noise, the obtained covariance should be considered as the phase noise of the modulator.
We made a comparison between single side band (SSB) phase noises of the multiplier and the Mach-Zehnder modulator signals using the SSB phase noise measurement system as shown in Fig. 8.

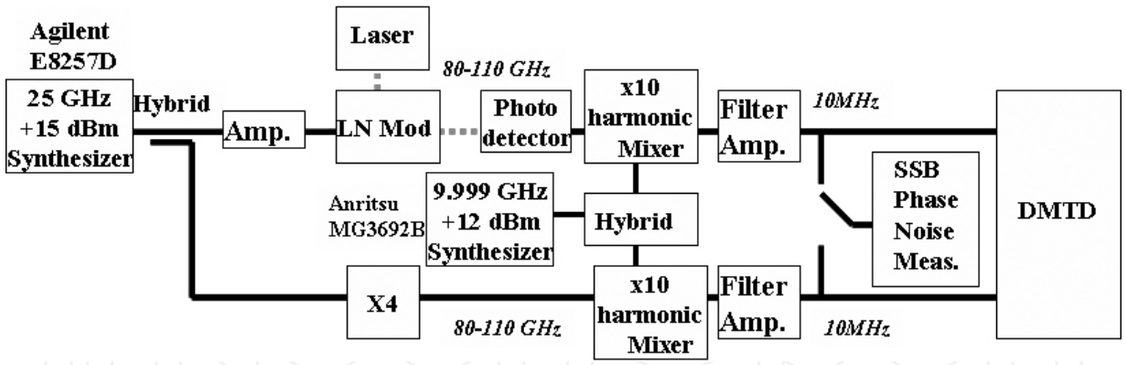

Fig. 8. Block diagram of a time-domain stability measurement system using the multiplier signal for the full-bias operation mode (the second-order optical modulation signal). This phase noise measurement system is free from the influence of reference signal phase noise and frequency conversion signal phase noise. This method is also regarded as a Dual-Mixer Time Difference method. The measured phase stability is the covariance of the Mach-Zehnder modulator and multiplier phase noises.

Since the current system doesn't have two identical LN modulators, we cannot perform the phase noise measurement between two identical LN modulators with the DMTD method. Consequently, it is meaningless to use the DMTD method if the phase noise of the multiplier to be compared is extremely bad.

The obtained results show at least the modulator has phase noise that is equivalent to or better than that of the multiplier in 1 kHz and higher frequency. The lower frequency phase noise is masked by the synthesizer phase noise. The measurement results of SSB phase noise is no more than a criterion for judgment of effectiveness of the measured Allan standard deviation with the DMTD method.

Phase stability of the Mach-Zehnder modulator measured using the Allan standard deviation is shown in Fig. 9. The stability is independent of the input laser line-width for a short fiber cable, the input lasers are a DFB-laser (10 MHz line-width) and a fiber-laser (1 kHz line-width).

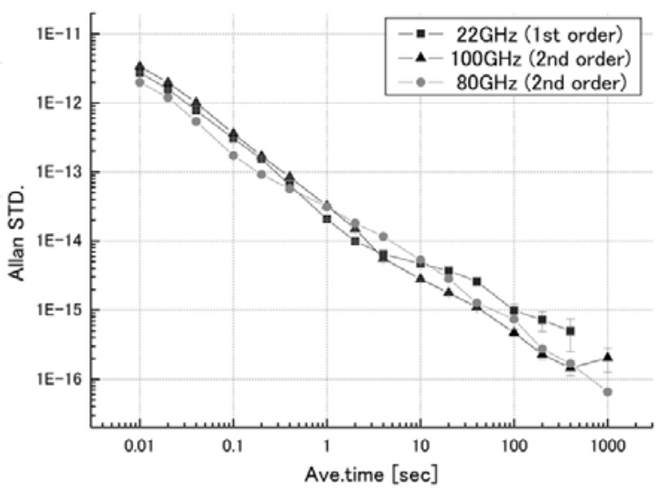

Fig. 9. Measured phase stabilities of the Mach-Zehnder modulator, the first-order 22 GHz signal and the second-order 100 GHz signal.

3.6 Differential polarization angle between two light-waves

The theme of this paper covers optical signal generation, but the ultimate goal of the photonic system is generation of highly-stable optical signal and its transmission with fiber system. The delay compensation must be performed on the delay caused during the optical signal transmission through an optical fiber cable in order to keep the signals coherent. In the photonic LO (Local) system, two optical signals are transmitted and converted by a photo mixer at a remote antenna into a microwave signal. During the signal transmission through the fiber cable, the cable length delay is caused, including Polarization Mode Dispersion (PMD), a bottleneck in performing successful phase compensation (delay change compensation). PMD is the state of polarizations (SOP) dispersing randomly in the cable. PMD is caused when the state of polarization of the two optical signals is absolutely changed by the movement of the cable through which the signals are transmitted. The magnitude of PMD is inversely proportional to the degree of the polarization alignment of the two optical signals. Since the generation of PMD contributes to the emergence of the Differential Group Delay (DGD) (synonymous with LO phase jitter), SOP of the two signals needs to be coincident so as to reduce the second order PMD effect on DGD.

We measured the differential polarization angle between two light-waves generated by the Mach-Zehnder modulator. The measurement block diagram is shown in Fig. 10. In this measurement, the two light-waves are transmitted to the ITU-Grid programmable optical filter (Peleton QTM050C), which selects one of the two light-waves for polarization. The polarization is measured by the polarization meter (Polarimeter). The differential angle is calculated by Eq. (12): spherical trigonometry.

$$\cos d = \sin\delta_1 \times \sin\delta_2 + \cos\delta_1 \times \cos\delta_2 \times \cos(\lambda_1 - \lambda_2) \tag{12}$$

The measured polarization angles in degrees are (δ_1: -29.2 in Azimuth, λ_1: -4.54 in Elevation) and (δ_2: -28.3, λ_2:-4.59). The calculated differential polarization angle: d is 0.90 degrees.

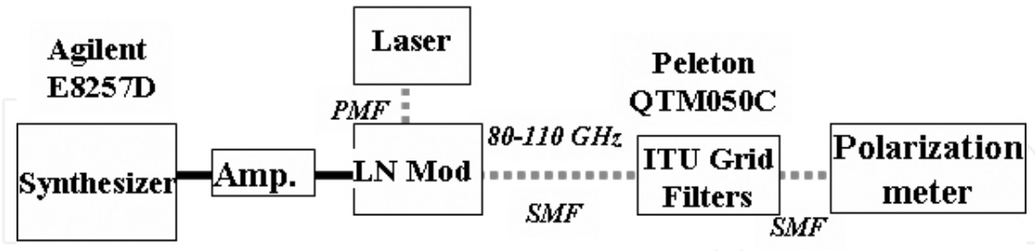

Fig. 10. Block diagram of the Polarization measurement. One of the two optical signals is selected by the ITU grid switch for polarization and transmitted to the Polarization meter.

3.7 Astronomical application

3.7.1 Estimated coherence loss

The measured stability of the null-bias point operation mode is 2.4×10^{-14} (white phase modulation noise) with 1.3×10^{-14} (white frequency modulation noise) at $\tau = 1$ sec, while the stability of the full-bias point operation mode is 3×10^{-14} (white phase modulation noise). With respect to a $\times n$ multiplier, multiplied phase noise (Vanblerkom & Aneman (1966)) should also be considered as shown below:

$$Multiplied\ \ phase\ noise$$

$$= Measured\ \ phase\ noise \times \sqrt{Multiplied\ number} \tag{13}$$

The coherence loss calculated from Equation (1) is smaller than 5% at the highest local frequency (938 GHz).
In the Dual-Mixer Time Difference system for the null-bias point operation mode shown in Fig. 7, phase noise of the measurement system (supposedly, white frequency modulation noise) is not canceled out as common noise, because the signal phase becomes unstable and incoherent in the amplification process by the AMP in the figure. The mild peak in 22 GHz around 30 seconds is thought to be due to white frequency modulation noise or instability of the amplifier, as the similar peak is not detected in the full-bias point operation (80 and 100 GHz measurements). Assuming the white frequency modulation noise is caused by any component other than the Mach-Zehnder Modulator, the phase noise of the Mach-Zehnder Modulator will be $\sigma_y(\tau = 1) = 2.4 \times 10^{-14}$. In this case, the coherence loss due to the phase noise will be constant, because the loss due to white phase modulation noise is independent of integration time. However, even if both of these noises are considered, the Mach-Zehnder modulator is still applicable to the most advanced systems such as ALMA and Very Long Baseline Interferometer (VLBI). The photonic millimeter-wave generator has been authorized as the MZM-LS (Mach-Zehnder Modulator scheme Laser Synthesizer) in ALMA project.

4. Round-trip phase stabilizer

Reference microwave signal or reference laser signal transfer via optical fiber have been researching in many fields (Sato et al. (2000), Daussy et al. (2005), Musha et al. (2006), Foreman et al. (2007)).

4.1 Basic concept of the round-trip phase stabilizer

Figure 11 shows the basic concept of the round-trip phase stabilizer(Kiuchi (2008)) for the two coherent-optical-signals. The optical signals are transmitted in one single-mode fiber. Under the effect of polarization mode dispersion (PMD), the transmission line lengths (the length of the signal path in the optical fiber cable) are different between the two coherent-optical-signals which are transmitted as a set.
The phase of these signals (λ_1 and λ_2 in wavelength) at the starting point of the roundtrip transmission is assumed to be zero, and the phase of these signals which have returned to the starting point are obtained from the following equations: $[(2\pi m) + \phi_1]$ for λ_1, and $[(2\pi m)+\phi_1 +2\Phi]$ for λ_2, respectively, where m and n are integers and Φ is the variable which is controlled by a phase shifter. The signal phase at the middle point of the roundtrip transmission (at the other end of the fiber) can be expressed as follows: For λ_1, $(\phi_1/2)$: m is even or $[(\phi_1/2) + \pi]$: m is odd, and: For λ_2, $[(\phi_2/2) + \Phi]$: n is even or $[(\phi_2/2) + \pi + \Phi]$: n is odd. Therefore, the transmitted signal phase is $(\phi_1/2)-[(\phi_2/2)+\Phi]$ or $(\phi_1/2)-[(\phi_2/2)+\Phi]+\pi$.
If we adjust the phase Φ as follows;

$$\phi_1 = \phi_2 + 2\Phi. \tag{14}$$

the signal phase at the antenna is the same as or just π different from the signal phase at the starting point of the roundtrip transmission.

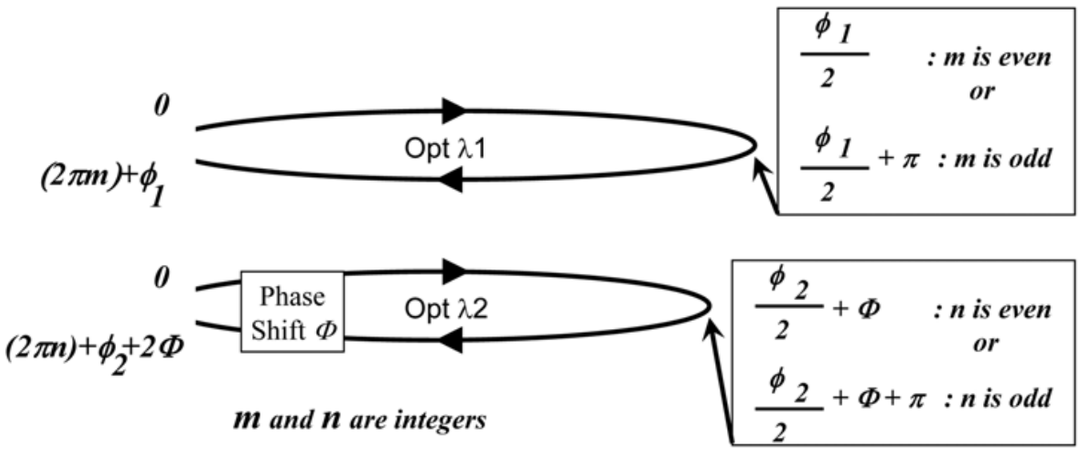

Fig. 11. Basic concept of the round-trip phase stabilizer. The two coherent-optical-signals (λ_1 and λ_2) are transmitted in one single-mode-fiber. Under the effect of PMD, the transmission line lengths (the length of the signal path in the optical fiber cable) are different between the two coherent-optical-signals. The effect of PMD will be expressed in this figure.

4.2 Round-trip optical dual-differential phase measurement scheme

The basic configuration of the system is shown in Figure 12. Signals generated by the two coherent-optical-signals generator in the previous section (Kawanishi et al. (2007),Kiuchi et al. (2007)) are sent to the antennas from the base-station (ground unit), together with PMD

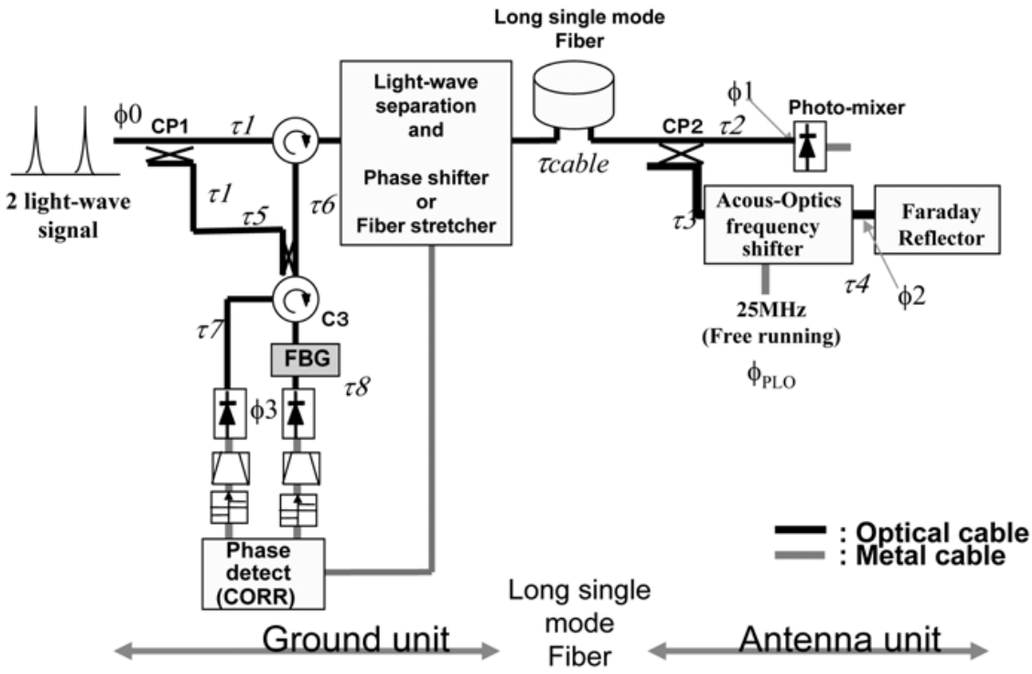

Fig. 12. The round-trip optical phase measurement scheme of the round-trip phase stabilizer.

caused by the rotation and coupling of the fiber cross section signals. At each antenna, frequency-shift modulation (ϕ_{PLO}, angular frequency is ω_t) is performed by the Acoust-Optics frequency shifter for the received optical signals which are then reflected by the optical reflector and returned to the shifter. The signals pass through one path in transmission. The frequency shift modulation is used to distinguish the round-trip signal from back-scattered signals. The phase difference between the signal at the starting point of the roundtrip transmission and the returned signal is detected by Michelson's interferometry to perform correlation of the orthogonal signals which are generated by a 90-degree phase shift of $2\omega_t$ (50 MHz). These orthogonal signals are not required for the phase-lock to the modulation signal at the antenna. Since the modulation frequency ($2\omega_t$) is small, its PMD (the second order PMD) can be ignorable (the estimated deviation value is shown in the next subsection). The round-trip phase measurement method is helpful for successful delay compensation of the microwave signal which is converted from the two coherent-optical-signals by a photo mixer.
In this method, a Faraday-reflector or a mirror both can be used as the reflector at the antenna. In the case of the Faraday reflector, the route of the transmitted and return of light are not completely corresponding. This difference becomes a fixed phase offset. However, the change of the phase offset can be compensated by the phase locked loop. The fixation phase offset does not influence the transmitted phase stability. In the case of using the Faraday rotator and a polarization splitter, it becomes advantageous with respect to the carrier noise ratio. The influence such as back-scattering can be reduced by separating polarization.

4.2.1 Polarization mode dispersion (PMD)

Polarization mode dispersion (PMD) (Agrawal (2002),Derickson (1998)) is the state of polarizations dispersing randomly in the cable. PMD arises from the anisotropic nature of the fiber cross section (θ_x and θ_y). PMD mainly consists of two components 1st and 2nd-order terms. The 1st-order component is differential group delay (DGD), and the 2nd-order components are polarization chromatic dispersion. In contrast to group velocity dispersion, PMD shows temporal change. PMD is caused when the state of polarization of the two coherent-optical-signals is absolutely changed by the movement of the cable through which the signals are transmitted.
We introduce two equations (Eqs. (15) and (17). The variance of differential group delay (Agrawal (2002), Derickson (1998)), can be approximated to be

$$\sigma_\tau = D_p L \tag{15}$$

Where Dp is the fiber PMD parameter of the optical fiber cable [$ps/\sqrt{km}$], and L is the cable length [km]. The variation of the delay will have a standard deviation of 39 fs (15 km fiber) if we choose a fiber with the lowest PMD of 0.01 $ps/\sqrt{km}$.
Second order PMD is the wavelength dependence of the propagation delay in the different polarization modes. The birefringence of the optical fiber cable is wavelength dependent; different wavelengths will cause different types of PMD. The deviation of the propagation delay caused by the second order PMD is as follows (Ciprut et al. (1998));

$$D_2 = \frac{2\pi c D_p^2}{\lambda^2 \sqrt{3}} \Delta_\lambda L \tag{16}$$

Where Δ_λ is the frequency difference between the two coherent-optical-signals. The deviation of the propagation delay caused by the second PMD is calculated as

$$\sigma_{\tau 2} = D_2 \times \Delta_{\lambda max} \times L_{max}. \tag{17}$$

DGD is calculated as the co-variance of the two deviations of the propagation delay. The maximum differential frequency of the two coherent-optical-signals is Δ_{max} = 1.1 *nm*. And when the L_{max} is 15 km, $\sigma_{\tau 2}$ is 0.74 fs.

In the case of the conventional technologies (Cliche & Shillue (2006)), as the round-trip measurement is performed with either one of the two optical signals, the delay on the two signals are compensated commonly by the fiber stretcher using the delay of the measured signal only. On the other hand, in the basic concept of the proposed system (Figures 11 and 12), the delays (σ_τ and $\sigma_{\tau 2}$) of the two signals are considered. The group delay σ_τ acts like a common mode noise to the two coherent-optical-signals. In addition, the round trip delays of the two coherent-optical-signals are measured and compensated independently, taking the differential delay between two coherent-optical-signals into consideration (Figure 11).

4.2.2 Phase relational expression

Firstly, for the phase relationship of the signals in one of the two coherent-optical-signals in Figure 11, the instrumental delay analysis is shown in Figure 12. The suffixes of the equations (λ1 and λ2) indicate the optical wavelength.

The phase of the optical signal to be transmitted from the two coherent-optical-signals generator is defined as $\phi_0(t)$.

$$\phi_0(t) = \omega_{\lambda 1}(t) + \phi_{\lambda 1}, \tag{18}$$

Where $\omega_{\lambda 1}$ is optical angular frequency, t is time, and $\phi_{\lambda 1}$ is initial/offset phase. If the time delay caused in the roundtrip signal transmission through the optical fiber cable is assumed to be τ_1, τ_{cable} (Figure 12), the received signal phase at the antenna is expressed as $\phi_1(t)$, at the point of the photomixer at antenna.

$$\phi_1(t) = \omega_{\lambda 1}(t - \tau_1 - \tau_{cable} - \tau_2) + \phi_{\lambda 1} \tag{19}$$

At the antenna, the received signals are modulated (frequency-shifted) by a microwave signal ϕ_{PLO} (25 MHz) and sent back to the ground unit through the optical cable.

$$\phi_{PLO}(t) = \omega_c(t) + \phi_c, \tag{20}$$

Where ω_c is a shift angular frequency (25 MHz), and ϕ_c is an initial phase. Frequency-shift of $\phi_{PLO}(t)$ is done by the Acoust-Optics frequency shifter. The signal phase at the reflector on the antenna is as follow;

$$\phi_2(t) = (\omega_{\lambda 1} + \omega_c)t - \omega_{\lambda 1}(\tau_1 + \tau_{cable} + \tau_3 + \tau_4)$$

$$-\omega_c\tau_4 + \phi_{\lambda 1} + \phi_c \tag{21}$$

The signal is reflected by an optical reflector, and returned to the ground-unit via the same cable in reciprocal process.

Differential phase between transmission and reception signals is measured by the Michelson's interferometer. The above equation is established assuming that the signal ($\lambda 1$) is reflected by Fiber Brag Grating (FBG1) and is converted into microwave ϕ_3 by the low-frequency photo mixer to detect $2\omega_t$. The frequency ($2\omega_t$) is selected by a microwave band pass filters.

$$\phi_3(t) = 2\omega_c(t) - \omega_{\lambda 1}(2\tau_{cable} + 2\tau_3 + 2\tau_4 + \tau_6 - \tau_5)$$
$$-2\omega_c(\tau_{cable} + \tau_3 + \tau_4 + \tau_6 + \tau_7) + 2\phi_c \quad (22)$$

This equation means that the roundtrip delay is measured as the optical differential phase of the frequency ($c/\lambda 1$, c: speed of light) after being converted to a microwave angular-frequency ($2\omega_t$).

Secondly, the phase relationship of the other optical signal ($\lambda 2$) can be obtained in conformity with Eqs. (18) to (22). When we use the two coherent-optical-signals, the cable delay is different between $\lambda 1$ and $\lambda 2$ under the effect of PMD. In the following equations, the cable delay in $\lambda 2$ is shown with hat. Initial optical ($\lambda 2$) signal is as follows:

$$\hat{\phi}_0(t) = \omega_{\lambda 2}(t) + \phi_{\lambda 2}, \quad (23)$$

The phase of the optical signal at the antenna is expressed as $\hat{\phi}_1(t)$.

$$\hat{\phi}_1(t) = \omega_{\lambda 2}(t - \hat{\tau}_1 - \hat{\tau}_{cable} - \hat{\tau}_2) + \phi_{\lambda 2} \quad (24)$$

The optical modulation is performed simultaneously for the wavelength of the two signals ($\lambda 1$ and $\lambda 2$) at the antenna, assuming that the optical signal passes through FBG1 and detected as microwave $\hat{\phi}_3(t)$ by the other photo mixer.

$$\hat{\phi}_3(t) = 2\omega_c(t) - \omega_{\lambda 2}(2\hat{\tau}_{cable} + 2\hat{\tau}_3 + 2\hat{\tau}_4 + \hat{\tau}_6 - \hat{\tau}_5)$$
$$-2\omega_c(\hat{\tau}_{cable} + \hat{\tau}_3 + \hat{\tau}_4 + \hat{\tau}_6 + \hat{\tau}_8) + 2\phi_c \quad (25)$$

This equation also means that the roundtrip delay is measured as the optical differential phase of the frequency ($c/\lambda 2$) which is then converted to a microwave angular-frequency $2\omega_t$.

Thirdly, Eq.(26) shows how to obtain the differential phase between $\phi_0(t)$ and $\hat{\phi}_0(t)$ at the starting point of the roundtrip transmission (with the single mode fiber long cable over 10 km).

$$\phi_0(t) - \hat{\phi}_0(t) = \omega_{\lambda 1}(t) - \omega_{\lambda 2}(t) + \phi_{\lambda 1} - \phi_{\lambda 2}, \quad (26)$$

In Eq. (27), the differential phase between $\phi_1(t)$ and $\hat{\phi}_1(t)$ is that of the signal received at the antenna.

$$\phi_1(t) - \hat{\phi}_1(t) = [\omega_{\lambda 1}(t) - \omega_{\lambda 2}(t) + \phi_{\lambda 1} - \phi_{\lambda 2}]$$
$$-\omega_{\lambda 1}(\tau_1 + \tau_{cable} + \tau_2) + \omega_{\lambda 2}(\hat{\tau}_1 + \hat{\tau}_{cable} + \hat{\tau}_2) \quad (27)$$

Comparing Eqs. (26) and (27), it is clear what comprises the instrumental delay. The equation for the phase change (ϕ_d) of the two optical signals caused in the transmission is as follows;

$$\phi_d = -\omega_{\lambda 1}(\tau_1 + \tau_{cable} + \tau_2) + \omega_{\lambda 2}(\hat{\tau}_1 + \hat{\tau}_{cable} + \hat{\tau}_2). \tag{28}$$

On the other hand, half of the differential phase between $\phi_3(t)$ and $\hat{\phi}_3(t)$, or the double-difference between the signals before/after the roundtrip transmission is as follows;

$$\frac{\phi_3(t) - \hat{\phi}_3(t)}{2} = -\omega_{\lambda 1}(\tau_{cable} + \tau_3 + \tau_4 + \frac{\tau_6 - \tau_5}{2})$$

$$+\omega_{\lambda 2}(\hat{\tau}_{cable} + \hat{\tau}_3 + \hat{\tau}_4 + \frac{\hat{\tau}_6 - \hat{\tau}_5}{2})$$

$$-\omega_c(\tau_{cable} + \tau_3 + \tau_4 + \tau_6 + \tau_7$$

$$-\hat{\tau}_{cable} - \hat{\tau}_3 - \hat{\tau}_4 - \hat{\tau}_6 - \hat{\tau}_8). \tag{29}$$

If this differential phase is compensated, the coherent transmission from the ground unit to the antenna can be realized. To compare Eq. (28) and Eq. (29), the term $(-\omega_{\lambda 1}\tau_{cable} + \omega_{\lambda 2}\hat{\tau}_{cable})$ is compensated by Eq. (29) (measured data).
The residual phase in this method is as follows:

$$Residual\ phase =$$

$$-\omega_{\lambda 1}(\tau_3 + \tau_4 + \frac{\tau_6 - \tau_5}{2}) + \omega_{\lambda 2}(\hat{\tau}_3 + \hat{\tau}_4 + \frac{\hat{\tau}_6 - \hat{\tau}_5}{2}) \tag{30}$$

$$-\omega_c(\tau_{cable} - \hat{\tau}_{cable} + \tau_3 - \hat{\tau}_3 + \tau_4 - \hat{\tau}_4 + \tau_6 - \hat{\tau}_6) \tag{31}$$

$$-\omega_c(\tau_7 - \hat{\tau}_8). \tag{32}$$

Lastly, the meanings of these equations are described below.
Eq.(30) shows the second order PMD of the cable whose length is $(\tau_3 + \tau_4 + (\tau_6 - \tau_5)/2)$,
Eq.(31) shows the ω_t(25 MHz) phase drift equivalent to the second order PMD of the cable length obtained by $(\tau_{cable} + \tau_3 + \tau_4 + \tau_6)$,
Eq.(32) shows the ω_t (25 MHz) phase difference equivalent to the phase drift of the cable length obtained by $(\tau_7 - \hat{\tau}_8)$.
Equations (30) and (32) are ignorable: the change of the differential delay is ignorable, because the length of $[\tau_3, \tau_4, \tau_5, \tau_6, \tau_7\ and\ \tau_8]$ is a few meters and not long enough to cause problems. Equation (31) is almost equal to Eq. (33).

$$\omega_c(\tau_{cable} - \hat{\tau}_{cable}) \tag{33}$$

This value is the inevitable error of this method. According to the Equations (15) and (17), the offset frequency in the round-trip signal ($2 \times \omega_t$=50 MHz) is $\Delta_{\lambda offset}$ = 0.0004 *nm*. The deviation of the propagation delay $\sigma_{\tau 2}$ is less than 0.003 fs, which is very small.

In the process, the effect of the first and second order PMD can be reduced by using double-difference of the independently measured phases of two optical signals of round-trip measurement.
As a result, we can measure the instrumental delay phase (twice of the cable delay phase). Moreover, this method does not require the transmission of the modulation signal (ω_t), which means we do not have to consider any phase delay of the modulation signal (ω_t). The measured phase is used to compensate the instrumental delay change and phase change.

4.3 Two optical signal separation and optical phase control scheme

If we use a fiber stretcher that stretches the two signals together and performs phase shift on both of them, it is hard to get an enough dynamic range of the phase shift. On the other hand, in our basic concept (Fig. 11) using a phase shifter (General Photonics FPS-001) instead of the fiber stretcher, the phase shift is performed on only one of the two optical signals (λ_1 and λ_2). Figure 13 shows the execution example. Transmission delay on the fiber is measured as the differential phase of the optical round-trip delay of each lightwave signal. At first, the two coherent-optical-signals have a vertical and high-extinction ratio polarization. In a series of processing in the ground unit, the polarization is maintaining. The signal flow is shown in Figure 13.

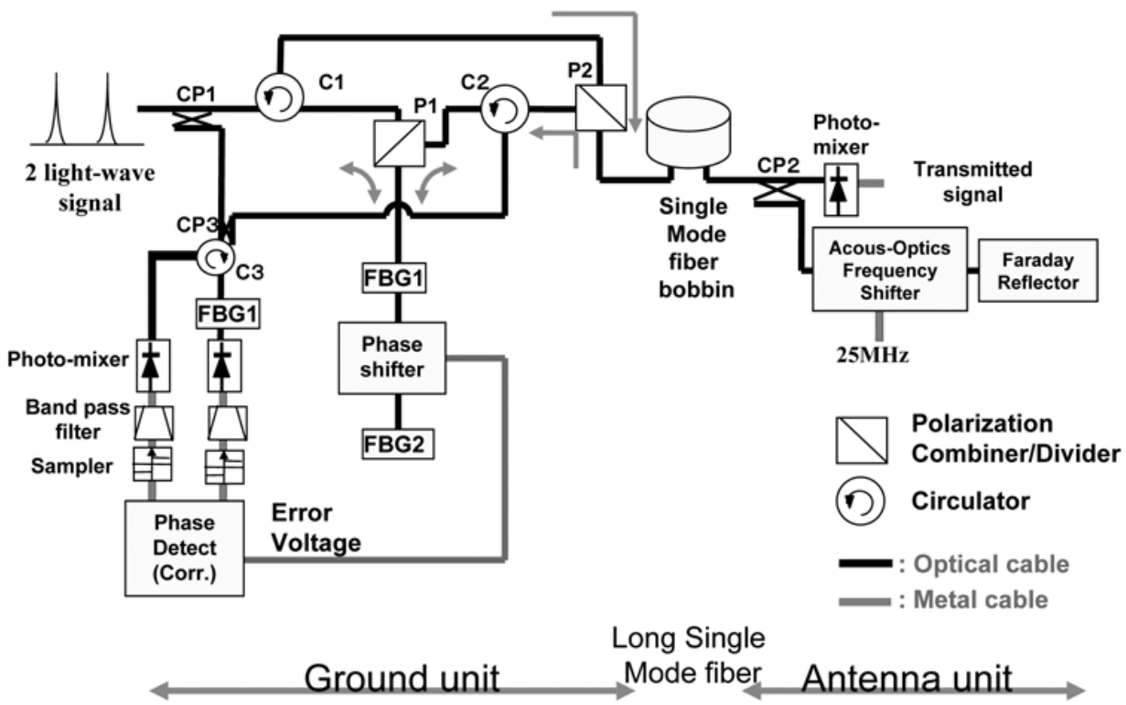

Fig. 13. Two optical signal separation and optical phase control scheme. Where CP1, CP2, CP3: optical coupler, C1, C2, C3: circulator, P1, P2: polarization beam splitter, and FBG1, FBG2: fiber bragg grating

The character in parentheses means an optical device in the figure. The signal, passing through the optical coupler (CP1), circulator (C1), and polarization beam splitter (P1), is divided into two wavelengths (λ_1 and λ_2). Wavelength λ_1 signal is reflected by a fiber bragg

grating (FBG1) and returned to the beam splitter (P1), while wavelength λ_2 signal is reflected by a fiber bragg grating (FBG2) and returned to the beam splitter (P1) via the phase-shifter. The returned light-waves are recombined at the beam splitter (P1) and sent to the circulator (C1), and then, to the polarization beam splitter (P2). The signal is divided into two signals at the optical coupler (CP2) after passing through a long single-mode fiber. One of the divided signals is converted to a millimeter wave by a photo-mixer, and the other signal is reflected by a Faraday reflector after the frequency shift by an optical frequency shifter (Acous-Optics frequency shifter). The reflected signal is converted into a 90-degree different optical polarization signal by the Faraday reflector. The signal, after passing through the frequency shifter again, is returned back to the polarization beam splitter (P2) in the ground unit. As the signal goes through the optical reciprocal process, the received signal has a horizontal (90-degree different polarization angle to the transmission signal) polarization at this point. After passing through the circulator (C2) and the beam splitter (P1), the signal is divided into two wavelengths (λ_1 and λ_2) again. As described above, wavelength λ_1 signal is reflected by the fiber bragg grating (FBG1) and returned to the beam splitter (P1), while wavelength λ_2 signal is reflected by FBG2 and returned to the beam splitter (P1) via the phase-shifter. The returned light-waves are recombined again at the beam splitter (P1) and sent to the circulator (C2) because the optical polarization is horizontal. And, finally the signal is recombined with the divided transmission signal at the optical coupler (CP3).

The differential phases on the angular frequency $2\omega_t$ between transmission and round-trip signals on each light-wave signal are detected by low-frequency photo-mixers after wavelength separation by the FBG1 optical filter (see previous Section). These measured phases are equivalent to the round-trip phases on both lightwave signals. In the proposed method, the transmitted signal will be stabilized by controlling the differential phase on the measurement signals to zero.

According to our experiments, a polarization controller is put into place between P1 and FBG1 produce a good effect.

4.4 Laboratory tests

A block diagram of the performance measurement system is shown in Figure 14. A set of the two coherent-optical-signals generated is divided into two signals: one is transmitted to the phase stabilizer system and the other to the photo mixer (Nippon Telephone and Telegraph (NTT) unitraveling-carrier photo-diode(Hirota et al. (2001),Ito et al. (2000))) as a reference signal. The signal passes through a 10-km Single-Mode Fiber cable with/without the phase stabilizer.

4.4.1 Phase stability measurements (Laboratory test)

We measured the phase stability (Fig. 15) of the transmitted signal (80 GHz) at the antenna through the single mode fiber cable (10 km) in the time-domain Allan STD method(Allan (1966), Allan (1976)) by a time interval analyzer: TSC-5110A. The measurements were conducted with/without the phase stabilizer to check the improvement of the phase stabilizer in the interferometric system.

When the optical signal (80 GHz) is transmitted through the single mode fiber cable (10 km), the phase stability begins to degrade around 10 seconds integration time. In the case of using the phase stabilizer, the degradation of the phase stability is staved off. The measured phase noise is the white phase noise.

Dynamic range of this method was measured by using a manual controlled air-gap stretcher which was inserted between the Ground unit and the single mode fiber spool in Figure 14. The measured dynamic range was larger than 5 cm.

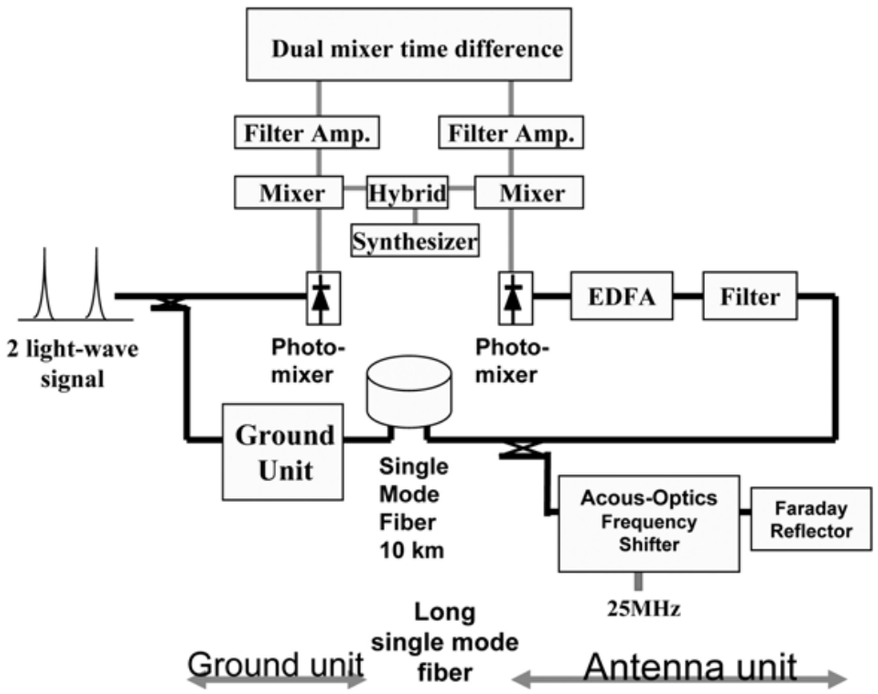

Fig. 14. A block diagram of phase stability measurement system. The signal is provided from the two coherent-optical-signals generator.

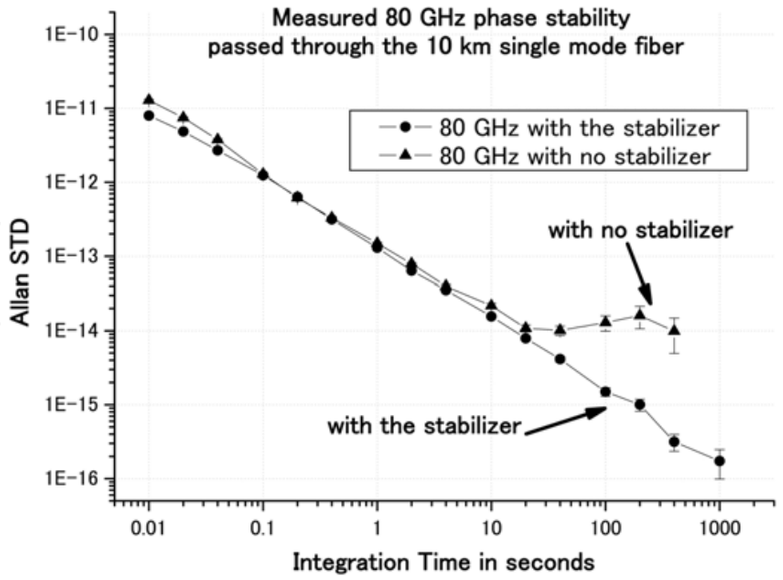

Fig. 15. The 80 GHz phase stability that passed through the 10 km fiber. The phase stability begins to degrade around 10 seconds integration time. In the case of using the phase stabilizer, the degradation of the phase stability is staved off.

4.4.2 Phase stability measurements (Field test)

In ALMA OSF (Operations Support Facility: 2900m sea level), there are built-up antennas and a Holography system which measures the antenna surface accuracy. The Photonic system field test was carried out using the Holography signal and two antennas (Antenna-1 and Antenna-4). The experiment block diagram is shown in Figure 16. The Holography transmitter, Antenna-2, Antenna-1 and Antenna-4 are standing in a low. Therefore the received Holography signals at Anttena-1 and Antenna-4 are blocked by Antenna-2, the received Holography signal levels are very weak. However Anttena-1 and Antenna-4 can receive the Holography signal simultaneously.

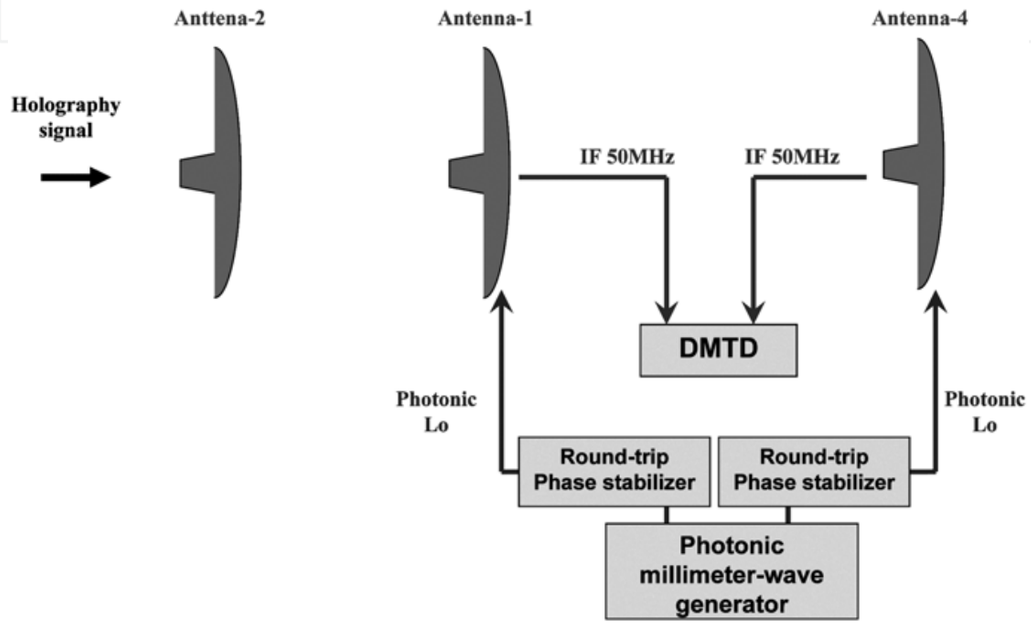

Fig. 16. Block diagram of the phase stability measurement experiment with the Holography transmitter. The Holography transmitter faces Antenna-2, with Antenna-1 and Antenna-4 aligned behind antenna-2. Two antennas can receive the Holography signal simultaneously.

In this experiment, the Holography signal was the common signal. Differential phase of Holography signal between Anttena-1 and Antenna-4 was measured. Received Holography signals (104.02 GHz) were converted down to intermediate frequency (IF: 50 MHz) signals by using the provided photonic signal from the Photonic millimeter-wave generator via the Round-trip phase stabilizer. The differential signal phase of these 50 MHz signals are measured by DMTD method. The measured phase stability is shown in Figure 17. The phase noise of 10^{-13} in White-PM noise was obtained, which is the covariance phase noise of two antenna system.

4.5 Verification results

In the ALMA Specification, instrumental delay/phase error on the 1st Local oscillator should be 53 fs (rms) in the short term, and long term drift should be 17.7 fs between 10 sec averaging at intervals of 300 seconds: $\sigma_y(1\ sec) < 9.2 \times 10^{-14}$. On the other hand, in the very long baseline interferometer (Rogers & Moran (1981), Rogers et al. (1984)) (VLBI), the requirements of 320 GHz are as follows: $\sigma_y(1\ sec) < 2 \times 10^{-13}$, $\sigma_y(100\ sec) < 1.3 \times 10^{-14}$ and $\sigma_y(1000\ sec) < 3 \times 10^{-15}$.

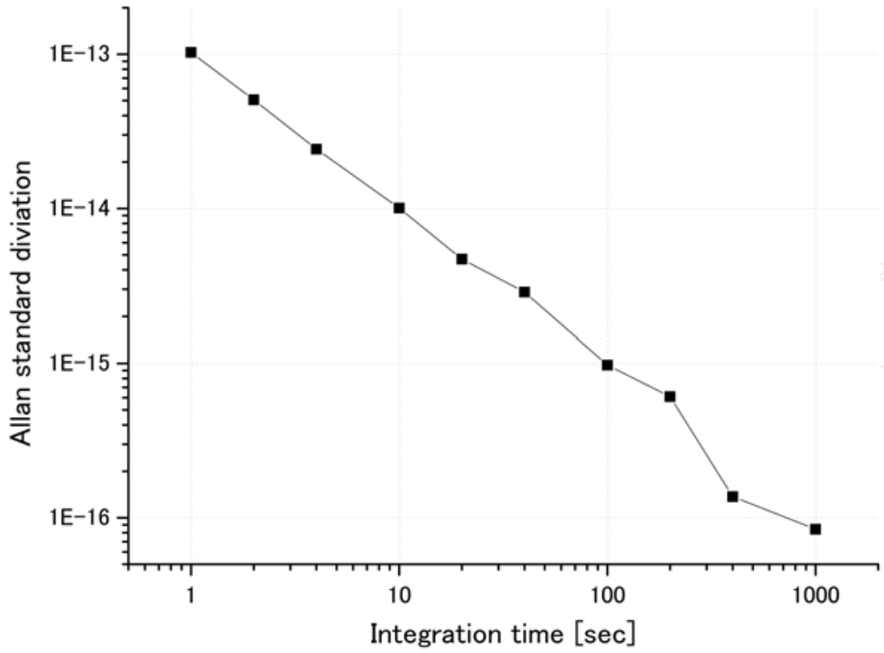

Fig. 17. The measured phase stability is measured by DMTD. The measured stability shows the co-variance of two antenna system stability. Received Holography signal (104.02 GHz) was converted down to 50 MHz by using the provided photonic signal from the Photonic millimeter-wave generator via the Round-trip phase stabilizer.

The verifications matrix is shown in Table 2. The measured values meet the ALMA specifications.

ALMA Specifications	Measured Values
53 fs (rms) in short-term 17.7 fs in long-term	42 fs (short) 13 fs (long)
Required Phase stability for VLBI $\sigma_y(1sec) < 9.2 \times 10^{-14}$ $\sigma_y(100sec) < 1.3 \times 10^{-14}$ $\sigma_y(1000sec) < 3 \times 10^{-15}$	Measured Phase stability $\sigma_y(1sec) < 7.3 \times 10^{-14}$ $\sigma_y(100sec) < 1.79 \times 10^{-15}$ $\sigma_y(1000sec) < 2.29 \times 10^{-16}$

Table 2. Verifications matrix.

5. Conclusion

Based on our experiment results, we propose a new high carrier suppression optical doublesideband intensity modulation technique using the integrated $LiNbO_3$ Mach-Zehnder modulator which is capable of compensating the imbalance of the Mach-Zehnder arms with a pair of active trimmers (null-bias operation mode). The full-bias point operation mode introduced in this paper is also a novel modulation technique for the second-order harmonic generation. The Mach-Zehnder modulator can generate two coherent light waves with frequency difference equivalent to four times the modulation frequency. Photonic local signals of 120GHz can also be generated using this technique.

The two spectral components of the two optical signals generated with this technique are phase-locked without using any complicated feedback control. All of the measurements were carried out on a table (without vibration isolation) in a normally air-conditioned room without acoustic noise isolation. In short, all of the measurements were performed under normal environment. Temperature change and mechanical vibrations may have affected the output lightwaves to some degree, however there was no chaotic phenomenon such as mode hopping or mode competition during the experiments. Based on these results, we concluded that the proposed techniques will be useful to construct a robust, low-cost and simple setup for the photonic local signals.

Compensation of the Local signal transmission delay is an indispensable technique for accurate interferometrical observation. PMD delay, which is caused during the signal transmission, needs to be reduced because it deteriorates the accuracy of the delay amount by affecting the signal polarization and wavelength. The two coherent-optical-signals generator (Kawanishi et al. (2007), Kiuchi et al. (2007)) is required to help stabilization of polarization, and to maintain the high extinction ratio, and to keep the signal state of polarizations in stable condition for preventing the delay generation.

We proposed the double difference phase measurement method. The method is also available to use the fiber stretcher instead of the phase shifter. The Double-difference method is more robust to external influences and more accurate than the current scheme which uses one of the two optical signals for measurement. This method can reduce deterioration in the signal phase stability caused by the long fiber signal transmission.

The performance advantages of the system are:

1. The modulation signal (ω_t) transmission and its phase compensation are not required (the modulation signal on the antenna is generated by a free-running oscillator);
2. External noise (acoustic noise, vibration noise) on the long single mode fiber cable is dealt with a common noise; and
3. The PMD problems are reduced, as the round trip delays on the two optical signals are measured and compensated independently.

6. References

Alferness,R.C.(1982), Waveguide electro-optic modulators, *IEEE Trans. Microw. Theory Tech.*, vol.30, no.8, pp.1121-1137.

Agrawal,G.P.(2002), *Fiber optic communication system, third edition*, JohnWiley & Sons Inc.

Allan, D.W. (1966), Statistics of Atomic Frequency Standards, *Proc. IEEE*, vol.54, pp.221.

Allan, D.W.(1976), Report on NBS dual mixer time difference system (DMTD) built for time domain measurements associated with phase 1 of GPS, *NBS IR*, vol.75, pp.827.

Ciprut,P., Gisin,B., Gisin,N., Passy,R., Von der Weid,J.P., Prieto,F., & Zimmer,C.w.(1998), Second-order polarization mode dispersion: Impact on analog and digital transmissions, *IEEE Journal of lightwave technology*, vol.16, no.5, pp.757-771.

Cliche,J., & Shillue,B.(2006), Precision timing control for radioastronomy, maintaining femtosecond synchronization in Atacama Large Millimeter Array, *IEEE control system magazine*, pp.19-26.

Daussy,C., Lopez,O., Amy-Klein,A., Goncharov,A., Guinet,M., Chardonnet,C., Narbonneau, F., Lours,M., Chambon,D., Bize,S., Clairon,A., & Santarelli,G.(2005), Long-Distance Frequency Dissemination with a Resolution of 10^{-17}, *Physical review letters*, vol.94, 203904.

Derickson,D., *Fiber optics test and measurement*, Prentice Hall PTR.

Fonseca,D.D., Monteiro,P., Cartaxo,A.,V.,T., & Fujita,M.(2004), Single sideband demonstration using a four phase-modulators structure, *2004 IEEE/LEOS workshop on advanced modulation formats*, FC2.

Foreman,S.M., Ludlow,A.D., de Miranda,M.H.G., Stalnaker,J.E., Diddams,S.A., & Ye,J.(2007), Coherent optical phase transfer over a 32-km fiber with 1-s instability at 10^{-17}, *Physics review letters*,DOI:10.1103/PhysRevLett.99.153601.

Healey, D.J.III (1972), Flicker of frequency and phase and white frequency and phase; Fluctuations in frequency sources, *Proc. 25th Annu. Sympo. On Frequency Control (ASFC)*, pp.29-42.

Hirota,Y., Ishibashi,T., & Ito,H.(2001), 1.55-um wavelength periodic traveling-wave photodetector fabricated using unitraveling-carrier photodiode structures, *IEEE J. of Lightw. Technol*, vol.19, pp.11.

Ito,H., Furuta,T., Kodama,S., & IshibashiT.(2000), InP/InGaAs uni-travelling-carrier photodiode with 310 GHz bandwidth, *Electron. Lett.*, vol.38, no.21, pp.1809-1810.

Izutsu,M., Yamane,Y., & Sueta,T.(1977), Broad-band travering-wave modulator using $LiNbO_3$ optical waveguide, *IEEE J. Quantum Electron.*, vol.13, no.4, pp.287-290.

Izutsu,M., Shikamura,S., & Sueta,T.(1981), Integrated optical SSB modulator/frequency shifter, *J. Quantum Electron.*, vol.17, pp.2225-2227.

Jiang,Q., & Kavehrad,M.(1993), A Sub-carrier-Multiplexed Coherent FSK System Using a Mach-Zehnder Modulator with Automatic Bias Control, *IEEE/LEOS Photonics Tech. Let. Journal*, vol.5, no.8, pp.941-943.

Kawaguchi, N. (1983), Coherence loss and delay observation error in Very-Long-Baseline Interferometry, *J. Rad. Res. Labs.*, vol.30, no.129, pp.59-87.

Kawanishi,T., Sakamoto,T., Shinada,S., Izutsu,M., Higuma,K., Fujita,T., & Ichikawa,J.(2004a), $LiNb_3$ high-speed optical FSK modulator, *Electron. Lett.*, vol.40, pp.691-692.

Kawanishi,T., & Izutsu,M.(2004b), Linear single-sideband modulation for high-SNR wavelength conversion, *Photon. Technol. Lett.*, vol.16, pp.1534-1536.

Kawanishi,T., Kiuchi,H., Yamada,M., Sakamoto,T., Tsuchiya,M., Amagai,J., & Izutsu,M.(2005), Quadruple frequency double sideband carrier suppressed modulation using high extinction ratio optical modulators for photonic local oscillators, *MWP 2005*, PDP03.

Kawanishi,T., Sakamoto,T., Miyazaki,T., Izutsu,M., Fujita,T., Mori,S., Higuma,K., & Ichikawa,J. (2006), High-speed optical DQPSK and FSK modulation using integrated Mach-Zehnder interferometers, *Optics Express*, vol.14, no.10, pp.4496-4478.

Kawanishi,T., Sakamoto,T., & Izutsu,M. (2007), High-speed control of lightwave amplitude phase and frequency by use of electrooptic effect, *IEEE Journal of selected topics in quantum electronics*, vol.13, no.1, pp.79-91.

Kiuchi,H., Kawanishi,T., Yamada,M., Sakamoto,T., Tsuchiya,M., Amagai,J. & Izutsu,M.(2007), High Extinction Ratio Mach-Zehnder Modulator Applied to a Highly Stable Optical Signal Generator, *IEEE Trans. Microwave Theory and Techniques*, vol.55, no.9, pp.1964-1972.

Kiuchi,H.(2008), Highly stable millimeter-wave signal distribution with an optical round-trip phase stabilizer, *IEEE Trans. Microwave Theory and Techniques*, vol.56, no.6, pp.1493-1500.

Lim,C., Nirmalathas,A., Novak,D., & Waterhouse,R.(2000), Optimisation of baseband modulation scheme for millimeter-wave fibre-radio systems, *Electron. Lett.*, vol.36, pp.442-443.

Musha,M., Sato,Y., Nakagawa,K., Ueda,K., Ueda,A., Ishiguro,M., Robust and precise length stabilization of a 25-km long optical fiber using an optical interferometric method with a digital phase-frequency discriminator, *Appl. Phys. B*, vol.82, pp.555-559.

Onillon,B., Constant,S., & Llopis,O., Optical links for ultra low phase noise microwave oscillators measurement, *IEEE frequency control symposium*.

Rogers, A.E.E. & Moran, J.M. (1981), Coherence limits for very-long-baseline interferometry, *IEEE Trans. Instrum. Meas.*, vol.30, no.4, pp.283-286.

Rogers, A.E.E., Moffet, A.T., Backer ,D.C. & Moran, J.M. (1984), Coherence limits in VLBI observation at 3-millimeter wavelength, *Radio Science*, vol.19, no.6, pp.1552-1560.

Sakamoto,T., Kawanishi,T., & Izutsu,M.(2005), Optical minimum-shift-keying with external modulation scheme, *Opt. Exp.*, vol.13, pp.7741-7747.

Sato,K., Hara,T., Kuji,S., Asari,K., Nishio,M., & Kawano,N.(2000), Development of an ultra stable fiber optic frequency distribution system using an optical delay control module, *IEEE Trans. Inst. Meas.*, vol.49, no.1, pp.19-24.

Vanblerkom,R., & Aneman,S.,L.(1966), Considerations for the short term stability of frequency multiplication, *IEEE AES-2*, vol.1, pp.36-47.

Vegas Olmos,J.,J., Tafur Monroy,I., & Koon,A.M.J.(2003), High bit-rate combined FSK/IM modulated optical signal generation by using GCSR tunable laser sources, *Opt. Exp.*, vol.11, pp.3136-3140.

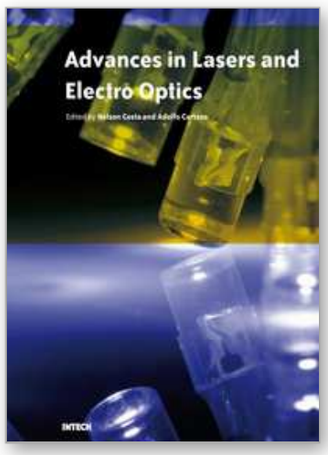

Advances in Lasers and Electro Optics

Edited by Nelson Costa and Adolfo Cartaxo

ISBN 978-953-307-088-9
Hard cover, 838 pages
Publisher InTech
Published online 01, April, 2010
Published in print edition April, 2010

Lasers and electro-optics is a field of research leading to constant breakthroughs. Indeed, tremendous advances have occurred in optical components and systems since the invention of laser in the late 50s, with applications in almost every imaginable field of science including control, astronomy, medicine, communications, measurements, etc. If we focus on lasers, for example, we find applications in quite different areas. We find lasers, for instance, in industry, emitting power level of several tens of kilowatts for welding and cutting; in medical applications, emitting power levels from few milliwatt to tens of Watt for various types of surgeries; and in optical fibre telecommunication systems, emitting power levels of the order of one milliwatt. This book is divided in four sections. The book presents several physical effects and properties of materials used in lasers and electro-optics in the first chapter and, in the three remaining chapters, applications of lasers and electro-optics in three different areas are presented.

INTECH
open science | open minds

InTech Europe
University Campus STeP Ri
Slavka Krautzeka 83/A
51000 Rijeka, Croatia
Phone: +385 (51) 770 447
Fax: +385 (51) 686 166
www.intechopen.com

InTech China
Unit 405, Office Block, Hotel Equatorial Shanghai
No.65, Yan An Road (West), Shanghai, 200040, China
中国上海市延安西路65号上海国际贵都大饭店办公楼405单元
Phone: +86-21-62489820
Fax: +86-21-62489821

IntechOpen